

ACADEMIC
PRESSAvailable online at www.sciencedirect.com

Journal of Sound and Vibration ■ (■■■■) ■■■-■■■

JOURNAL OF
SOUND AND
VIBRATIONwww.elsevier.com/locate/jsvi

A methodology for predicting impact-induced acoustic noise in machine systems

C.H. Oppenheimer*, S. Dubowsky

Department of Mechanical Engineering, Massachusetts Institute of Technology, Cambridge, MA 02139, USA

Received 30 August 1999; accepted 1 October 2001

Abstract

A methodology for predicting noise and vibration of machines and their support structures is presented. Included is a heuristic energy-based criterion to assess the importance of dynamic coupling between a mechanism and its support structure based on a simplified analysis of a mechanism operating on a rigid base, which neglects the coupling. Also included is an analysis method that considers the coupling and to be used when the criterion reveals important coupling. The methodology is implemented using highly idealized closed form and more elaborate numerical descriptions and is checked against vibration and sound measurements of a plate subjected to periodic impacts by balls and a beam that rattles within a clearance bearing. The energy-based criterion is found to indicate situations in which mechanism-support coupling affects noise radiation. In some cases the coupling is observed to significantly affect vibration and noise radiation of the support structure, while having a relatively minor effect on mechanism response. Both the simple closed form and numerical descriptions are found to predict noise trends due to variations in machine speed and bearing clearance, and the numerical descriptions more accurately predict overall and band levels of noise radiation.

© 2003 Elsevier Science Ltd. All rights reserved.

1. Introduction

This paper presents a methodology for predicting impact-induced noise produced by machine systems and their supporting structures. In many machine systems, noise is radiated from vibration of supporting structures and enclosures with large surface areas that are excited by the motion of the machine. In particular, impacts within clearances between the machine elements or the work, such as in punch presses or printers, can produce loud, high-frequency noise in this manner.

*Daly-Standlee & Associates, Inc., 4900 SW Griffith Drive, Suite 216, Beaverton, OR 97005, USA.

Noise prediction techniques are available for machine systems with linear dynamic behavior such as supporting structures. Finite Element and Boundary Element Analysis are well suited for low-frequency applications where a small number of system modes dominate the system response [1,2]. Statistical energy analysis (SEA) is a complementary method suited for high frequencies where a large number of modes participate in the system response [3,4]. Such linear methods do not well describe the non-linear dynamic behavior found in machine systems with large kinematic motions or impacts in connections with clearance or backlash. Moreover, techniques suited for machine systems with non-linear dynamic behavior do not readily accommodate supporting structures. Techniques that model the noise and vibration of mechanisms with distributed mass and flexibility, time-varying kinematic configurations, and impacts include the support structure with the heavy burden of time integrating the response of numerous support structure modes in the audible frequency range [5,6].

The methodology presented here targets machine systems consisting of mechanisms with non-linear behavior and their support structures. The methodology provides a general framework for predicting radiated noise and vibration, ranking noise contributions, and assessing noise trends due to varying system parameters based on physical principals. The intent is to make predictions useful to the practicing engineer based on design drawings. This means that overall radiated noise levels should be predicted within 3 dB, and the most accurate prediction of band levels should fall in the 500–10,000 Hz band emphasized by A-weighting, as A-weighted levels have been linked to hearing loss [7].

A valuable feature of the methodology is the ability to assess the importance of dynamic coupling between a mechanism and its support structure without simulating this coupling. This is accomplished using a heuristic energy-based criterion determined from the response of the mechanism operating on a rigid base. If the coupling is unimportant, the rigid base analysis serves as the basis for predictions of noise radiation. If the coupling is important, a coupled analysis that considers the dynamic coupling between the mechanism and support structure must be done before making acoustic predictions. In short, the heuristic coupling criterion uses a *decoupled* analysis to assess the importance of the coupling and the usefulness of the decoupled analysis for predicting noise radiation.

The methodology can be implemented using various modelling approaches, and two approaches are presented here. A simple closed form approach idealizes mechanisms as rigid members and describes support structures in terms of average multi-modal behavior. A more elaborate numerical approach describes the clearance connections, non-linear kinematics, and distributed mass and flexibility of mechanisms using ASSET [8], and uses a combination of elastic and modal average descriptions for support structures. Modal average descriptions are used because of the response variability of nominally alike structures [9,10]. The elastic-modal average combination provides a support structure description that can be coupled to a non-linear dynamic description of a mechanism to predict structural vibration and noise radiation over the audible spectrum.

Predictions by the methodology are compared to measured data for two systems. One system is a plate bombarded by steel balls; the other is a hinged beam that rattles within an instrumented clearance bearing. The energy-based criterion using rigid base analysis is found to indicate the importance of coupling between mechanism and support structure for both systems. Mechanism-support coupling is found to affect acoustic radiation significantly more than mechanism response

in the two systems considered. The simple closed form and more elaborate numerical modelling approaches are found to be comparable in predicting sensitivity of noise radiation to system parameters, and the numerical approach is found to be more accurate in predicting overall and band levels than the simple approach.

2. The noise prediction methodology

Impacts that occur in a machine's clearance connections and with the machine's work can excite vibrations in the machine, its support structure, and its enclosures. The vibrations in turn radiate noise. A machine system is partitioned into a mechanism and a support structure to model this process. The support structure can include machine enclosures. The mechanism may experience large displacements and arbitrary drive or impact forces. The support structure is restricted to small displacement vibrations. The mechanism and support structure interact dynamically at coupling nodes of the mechanism and ports of the support structure; see Fig. 1. Coupling of the two subsystems through the air is neglected. The mechanism is composed of links that may be assumed rigid or elastic. The nominal motion of the links is defined by a set of coordinates $\Theta = [\theta_1 \dots \theta_M]^T$. Perturbations of the links, due to joint motions within clearances and elastic motion of the links, from their nominal motions are described by a set of perturbation coordinates $\mathbf{q} = [q_1 \dots q_N]^T$ [8].

The support structure is represented by SEA subsystems. SEA subsystems are groups of similar modes, typically representing a geometrically idealized part of a linear dynamic system [3]. Adjacent subsystems are directly coupled to the mechanism at ports. Velocities at the ports are contained in a vector $\mathbf{v} = [v_1^T \dots v_{N_a}^T]^T$ in which the subscript denotes the adjacent support subsystem. Remote subsystems are excited into vibration by other subsystems and are indirectly coupled to the mechanism. Weak coupling is assumed between all subsystems, a standard SEA assumption.

A key feature of the methodology is the treatment of dynamic coupling between a mechanism and its support structure; see Fig. 2. First, a decoupled analysis of the mechanism operating on a rigid base is performed, which neglects the coupling. A heuristic energy-based criterion then

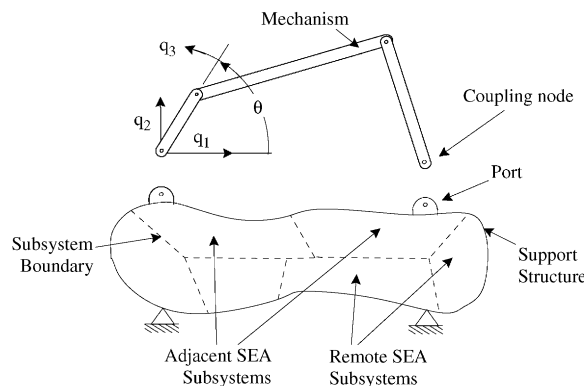


Fig. 1. A machine system model.

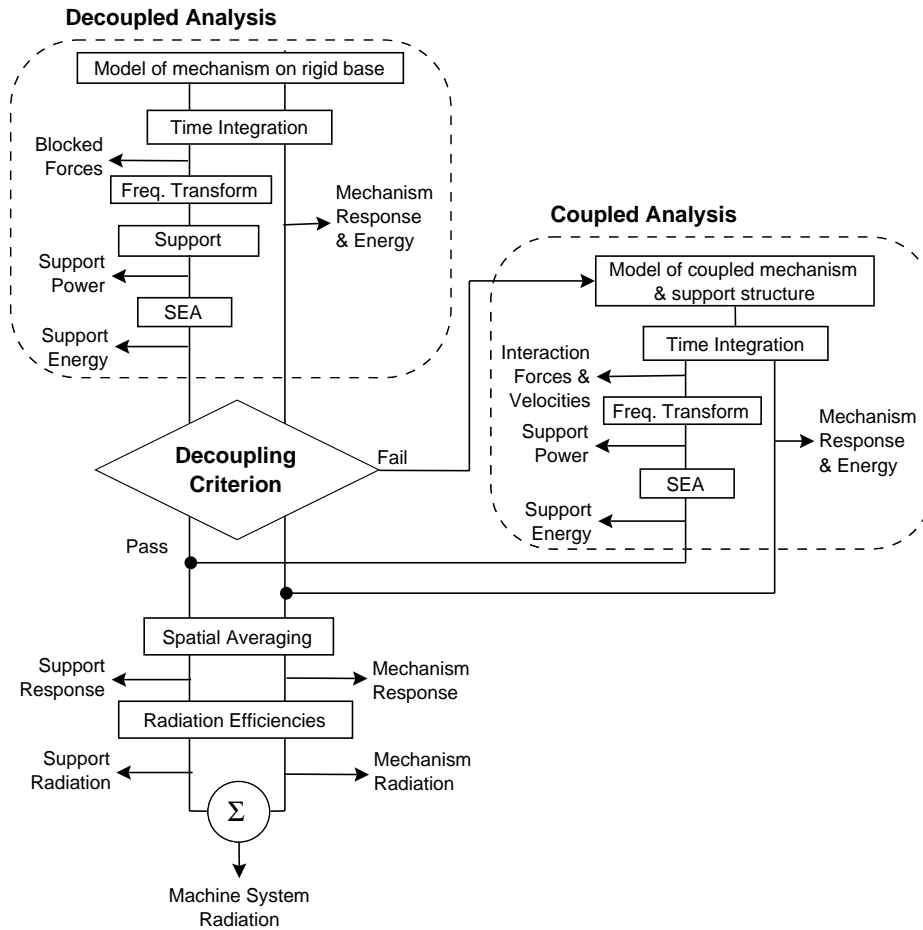


Fig. 2. Flowchart of methodology.

assesses the validity of the decoupled analysis, based on the results of the rigid base decoupled analysis. If deemed valid by the criterion, the results are used to determine sound radiation. If not, a coupled analysis that considers mechanism-support coupling is performed, and its results are used to determine sound radiation.

2.1. Decoupled analysis

As described above, analysis begins by neglecting the dynamic interactions between the mechanism and the support structure; see Fig. 2. The mechanism dynamic response is calculated with a flexible support structure replaced by a rigid base. The blocked coupling loads on the rigid base are then applied to the support structure in a separate linear dynamic analysis of the support structure. The general form of the equations of motion for the mechanism is

$$\mathbf{M}(\Theta)\ddot{\mathbf{q}} + \mathbf{G}(\Theta, \dot{\Theta})\dot{\mathbf{q}} + \mathbf{K}(\Theta, \dot{\Theta}, \ddot{\Theta})\mathbf{q} = \mathbf{Q}(\mathbf{q}, \dot{\mathbf{q}}, \Theta, \dot{\Theta}) \quad (1)$$

in which \mathbf{q} contains perturbation displacements of the links with respect to their motion, \mathbf{Q} contains generalized forces on the link nodes which describe impact, gravity, and mechanism driving forces, \mathbf{M} is a mass matrix, \mathbf{G} is an effective non-linear damping matrix describing structural damping and Coriolis effects, and \mathbf{K} is an effective non-linear stiffness matrix describing structural, centrifugal, and acceleration stiffness effects. The \mathbf{M} , \mathbf{G} , and \mathbf{K} are time-varying, non-linear matrices which depend on the configuration Θ of the mechanism. The mechanism description is obtained in this work using ASSET, which uses finite element descriptions of the links of a mechanism [8]; other mechanism dynamic modelling methods could be used as well.

It is convenient to partition Eq. (1) as follows:

$$\begin{bmatrix} \mathbf{M}^{II} & \mathbf{M}^{IC} \\ \mathbf{M}^{CI} & \mathbf{M}^{CC} \end{bmatrix} \begin{Bmatrix} \ddot{\mathbf{q}}^I \\ \ddot{\mathbf{q}}^C \end{Bmatrix} + \begin{bmatrix} \mathbf{G}^{II} & \mathbf{G}^{IC} \\ \mathbf{G}^{CI} & \mathbf{G}^{CC} \end{bmatrix} \begin{Bmatrix} \dot{\mathbf{q}}^I \\ \dot{\mathbf{q}}^C \end{Bmatrix} + \begin{bmatrix} \mathbf{K}^{II} & \mathbf{K}^{IC} \\ \mathbf{K}^{CI} & \mathbf{K}^{CC} \end{bmatrix} \begin{Bmatrix} \mathbf{q}^I \\ \mathbf{q}^C \end{Bmatrix} = \begin{Bmatrix} \mathbf{Q}^I \\ \mathbf{Q}^C \end{Bmatrix}, \quad (2)$$

where superscripts I and C denote internal and coupling partitions. A coupling node of a mechanism interacts with a support structure; an internal node does not. The equation of motion for a mechanism operating on a rigid base is found by setting the coupling perturbations \mathbf{q}^C to zero:

$$\mathbf{M}^{II}\ddot{\mathbf{q}}^I + \mathbf{G}^{II}\dot{\mathbf{q}}^I + \mathbf{K}^{II}\mathbf{q}^I = \mathbf{Q}^I. \quad (3)$$

The loads exerted on the rigid base by the mechanism are obtained during time integration using the internal perturbations and the cross coupling stiffness matrix:

$$\ell(t) = \mathbf{K}^{CI}\mathbf{q}^I. \quad (4)$$

The blocked loads $\ell(t)$ are indexed by the subsystems that they excite: $\ell(t) = [\ell_1(t) \dots \ell_{N_a}(t)]^T$, in which N_a is the number of adjacent support subsystems.

The response of the support structure is then found by applying the blocked forces to the support structure. The assumption of small displacements permits use of linear theory. The Fourier spectrum of the blocked forces $\ell(t)$ is obtained using spectrum estimation techniques [11]. The result is a vector of complex force components: $\tilde{\mathbf{L}}(\omega) = [\tilde{\mathbf{L}}_1^T(\omega) \dots \tilde{\mathbf{L}}_{N_a}^T(\omega)]^T$, in which the tilde indicates a complex quantity. The power delivered to each adjacent subsystem is then found by

$$\Pi_k^a(\omega) = \frac{1}{2}\text{Re}\{\tilde{\mathbf{L}}_k^H(\omega)\tilde{\mathbf{Y}}_k(\omega)\tilde{\mathbf{L}}_k(\omega)\}, \quad k = 1, \dots, N_a, \quad (5)$$

in which superscript H denotes conjugate transpose (Hermitian), Re is the real part operator, and $\tilde{\mathbf{Y}}_k$ is a mobility matrix containing ratios of complex velocity and force amplitudes for an adjacent subsystem. In using Eq. (5), the dynamic effects of coupling across subsystem boundaries have been neglected by the weak coupling assumption. The subsystem powers $\Pi_k(\omega)$ are aggregated in bands and excite a SEA model of the support structure. The energy in each support subsystem is then found by inverting the SEA equation [3]:

$$\omega\boldsymbol{\eta} \begin{Bmatrix} \mathbf{E}^a \\ \mathbf{E}^r \end{Bmatrix} = \begin{Bmatrix} \boldsymbol{\Pi}^a \\ 0 \end{Bmatrix}, \quad (6)$$

where $\boldsymbol{\eta}$ is a matrix of damping and coupling loss factors [3]. The vector $\mathbf{E}^a = [E_1^a(\omega_c) \dots E_{N_a}^a(\omega_c)]^T$ contains adjacent subsystem energies, $\mathbf{E}^r = [E_1^r(\omega_c) \dots E_{N_r}^r(\omega_c)]^T$ contains remote subsystem energies, and $\boldsymbol{\Pi}^a = [\Pi_1^a(\omega_c) \dots \Pi_{N_a}^a(\omega_c)]^T$ contains adjacent subsystem powers, all referenced to the analysis bands by center frequency ω_c . The zero vector of length N_r in Eq. (6) is present

because by assumption no power is delivered to remote subsystems by direct coupling with the mechanism. The SEA assumption of incoherent excitation across subsystems may be violated by coherent mechanism loads on the support structure; this assumption has often been violated in past work [3].

A variety of descriptions can be used for the support subsystem mobility matrix $\tilde{\mathbf{Y}}_k$ of Eq. (5). In this paper, elastic and modal average resonant descriptions are combined for a subsystem k ,

$$\tilde{\mathbf{Y}}_k = \left[\mathbf{K}_k / i\omega + \tilde{\mathbf{Y}}_{\infty,k}^{-1} \right]^{-1}, \quad (7)$$

in which the stiffness matrix \mathbf{K}_k describes elastic behavior and the mobility matrix $\tilde{\mathbf{Y}}_{\infty,k}$ describes the behavior of multiple resonant modes averaged over frequency and drive and response location. The modal average mobility matrix $\tilde{\mathbf{Y}}_{\infty,k}$ is most conveniently derived from an infinite system obtained by extending the finite subsystem to infinity in directions of wave propagation [12,3,13]. Eq. (7) expresses elastic behavior at low frequencies and resonant multi-modal behavior at high frequencies.

2.2. Coupling criterion

The rigid base decoupled analysis neglects the dynamic coupling between the mechanism and its support structure to greatly simplify the analysis, but it also reduces modelling accuracy. An energy-based criterion is evaluated to assess the decoupled analysis. The criterion compares the mechanism and support energies predicted by decoupled analysis. The mechanism and support are expected to be essentially decoupled from one another when

$$\frac{\langle E_{supp} \rangle}{\langle E_{mech} \rangle} < 1, \quad (8)$$

where $\langle E_{mech} \rangle$ is the energy of a mechanism operating on a rigid base and $\langle E_{supp} \rangle$ is the energy of the support structure resulting from application of blocked port forces; the brackets indicate an average taken over times when a blocked load on the rigid base is non-zero. The coupling criterion is motivated by the limiting case of a rigid support structure, which has zero energy. An appealing feature of the coupling criterion is its simplicity in dealing with non-linear configuration-dependent behavior. An impedance-based criterion would be more complicated, involving multiple comparisons at various mechanism configurations and link contact conditions. The energy of the mechanism is given by

$$\langle E_{mech} \rangle = \frac{1}{2} \langle \dot{\mathbf{q}}^T \mathbf{M}(\Theta) \dot{\mathbf{q}} \rangle + \frac{1}{2} \langle \mathbf{q}^T \mathbf{K}(\Theta, \dot{\Theta}, \ddot{\Theta}) \mathbf{q} \rangle, \quad (9)$$

in which the terms on the right-hand side are the kinetic and potential energies of the mechanism, and the configuration dependence has been made explicit. The support structure energy is

$$\langle E_{supp} \rangle = \sum_k E_k, \quad (10)$$

where E_k are the subsystem energies obtained by solving Eq. (6). The SEA solution provides the average support structure energy over the simulated operating time. If the loads on the rigid base are not continuous in time, the support energy is increased by the proportion of time during which loads are applied. If the coupling criterion of Eq. (8) is satisfied, the rigid base simulation is

deemed useful and is used to determine noise radiation. The time and surface averaged square of surface normal velocities $\langle v_l^2 \rangle$ of mechanism link l are found by suitable averaging. The mean square velocities of the support structure subsystems are given by $\langle v_k^2 \rangle = E_k/M_k$ in which M_k and E_k are the mass and energy of support subsystem k . Radiated sound power is then obtained by assuming that system components radiate independently:

$$\Pi = \rho_0 c \left(\sum_{links} \sigma_l S_l \langle v_l^2 \rangle + \sum_{support} \sigma_k S_k \langle v_k^2 \rangle \right), \quad (11)$$

in which ρ_0 and c are the density and speed of sound in air, S is radiating surface area, and σ is radiation efficiency. Independent radiation is approximated, for design purposes, when components are separated by more than one-tenth of an acoustic wavelength [4,14,15]. In addition, noise contributions by nominal mechanism motion and ejection of air from joint clearances have been omitted because they typically are negligible [5].

2.3. Coupled analysis

In the event that the coupling criterion of Eq. (8) is not satisfied, a more accurate coupled analysis is performed that considers interaction between the mechanism and its support structure. The adjacent subsystems of the support structure, which couple directly with the mechanism, are represented by impulse response functions, as permitted by the small amplitude displacement assumption. The effects of remote subsystems on interactions between the mechanism and support structure are neglected by the assumption of weak coupling between subsystems.

The steps in coupled analysis following time integration nearly mimic those of decoupled analysis, see Fig. 2. The only difference is that port forces and velocities are both available in coupled analysis and the power delivered to a support structure subsystem is

$$\Pi_k(\omega) = \frac{1}{2} \text{Re} \{ \mathbf{L}_k^H \mathbf{V}_k \}, \quad (12)$$

in which $\mathbf{L}_k(\omega)$ and $\mathbf{V}_k(\omega)$ are the Fourier force and velocity spectra for the ports of subsystem k , and superscript H denotes complex conjugate.

The adjacent support subsystems that couple directly with the mechanism may be represented as impedance or mobility elements. In the mobility representation, loads are imposed on the support structure, and the support structure responds with velocities. In the impedance representation, velocities are imposed on the support structure, and the support structure responds with loads. The choice between a mobility or impedance representation is based on analytical convenience. Impulse response functions for the mobility description are generally easier to derive because they follow directly from the equation of motion. In either case, causality must be preserved to time integrate machine system response: a support mobility element must interact with mechanism compliance or resistance, and a support impedance element must interact with mechanism inertia.

2.3.1. Support mobility representation

When a support subsystem is represented by a mobility element, a mechanism exerts generalized forces \mathbf{Q}^C against the support, producing port velocities in the support structure,

$$\mathbf{v} = \mathbf{y} \cdot \mathbf{Q}^C, \quad (13)$$

in which $\mathbf{y}(t)$ is a symmetric matrix containing “mobility response functions.” Since coupling between support subsystems is assumed weak, $\mathbf{y}(t)$ is a block diagonal matrix $\mathbf{y}(t) = \text{diag}(\mathbf{y}_1 \dots \mathbf{y}_{N_a})$ where $\mathbf{y}_k(t)$ is the mobility response matrix for adjacent support subsystem k that contains velocity responses to impulses of applied loads. The mobility response functions used in this paper combine elastic and modal average dynamic descriptions,

$$\mathbf{y}_k(t) = \frac{d}{dt} \mathbf{K}_k^{-1} \delta(t) + \mathbf{y}_{\infty,k}(t), \quad (14)$$

in which $\delta(t)$ is the Dirac Delta function, \mathbf{K}_k is a subsystem stiffness matrix, and $\mathbf{y}_{\infty,k}(t)$ is a matrix of modal average mobility response functions derived from the infinite system associated with the finite subsystem. When using the mobility representation, the ASSET equation, Eq. (1), is supplemented with an expression for the interaction forces \mathbf{Q}^C between a mechanism and its support structure:

$$\dot{\mathbf{Q}}^C = \begin{cases} -\mathbf{K}[\mathbf{y} * \mathbf{Q}^C + \mathbf{R}^{-1} \mathbf{Q}^C + \dot{\mathbf{q}}^C], & \mathbf{g}(\mathbf{Q}^C, \mathbf{q}^C - w, \delta) > 0, \\ 0, & \text{otherwise,} \end{cases} \quad (15)$$

in which \mathbf{q}^C contains mechanism coupling node displacements, $w = \int \mathbf{v} dt$ contains support port displacements, δ contains joint clearances, and matrices \mathbf{K} and \mathbf{R} describe elasticity and resistance between mechanism coupling nodes and support structure ports and have the same block diagonal structure as the mobility response matrix $\mathbf{y}(t)$. The symbol $*$ denotes the convolution operator. The function \mathbf{g} describes the joints between a mechanism and its support structure. For clearance joints, \mathbf{g} is a non-linear function that ensures that interaction loads are repulsive and occur during mechanism–support contact; examples can be found in Ref. [16]. The mobility support representation is used for the Ball Drop System described in Section 3.

2.3.2. Support impedance representation

When a support is represented using the impedance representation, the generalized forces \mathbf{Q}^C in the ASSET Equation, Eq. (2), are expressed as

$$\mathbf{Q}^C = \begin{cases} \mathbf{z} * \dot{\mathbf{q}}^C, & \mathbf{h}(\mathbf{q}^C) \geq \delta, \\ 0, & \text{otherwise,} \end{cases} \quad (16)$$

in which δ is a vector of joint clearances, \mathbf{h} is a function that describes the (possibly non-linear) joint between the mechanism and the support structure, and $\mathbf{z}(t)$ is a symmetric matrix of “impedance response functions” that describe the loads that develop in response to velocity impulse while all but the driven degree of freedom (d.o.f.) are held fixed. The matrix $\mathbf{z}(t)$ has the same block diagonal structure as the mobility response function matrix $\mathbf{y}(t)$. The impedance response functions used here combine elastic and modal average descriptions for subsystem k :

$$\mathbf{z}_k(t) = \mathbf{z}_{\infty,k}(t) + \int \mathbf{K}_k \delta(t) dt, \quad (17)$$

in which \mathbf{K}_k is a stiffness matrix, and $\mathbf{z}_{\infty,k}(t)$ is a matrix of modal average impedance response functions. The impedance support representation is used for the Impact Beam System described in Section 4.

3. The Ball Drop System

The Ball Drop System is a simple system that provides a first test for the noise prediction methodology. The Ball Drop System is pictured in Fig. 3. Balls are expelled periodically from a hopper by a reciprocating plunger and fall onto an inclined plate supported at its corners by elastic cords. The 9.53 mm diameter steel balls were expelled at a rate of 2 Hz and hit the plate with a normal velocity of 3.9 m/s. Two aluminum plates were used. Each are $0.4\text{ m} \times 0.32\text{ m}$ and with thicknesses 6.4 and 12.7 mm. Felt was applied to the back of the plates to provide damping. Loss factors of the fundamental plate modes were measured to be 0.012 for the 6.4 mm thick plate and 0.0055 for the 12.7 mm thick plate.

Sound power was experimentally obtained using the reverberant room method, which uses measurements of sound pressure and room decay to determine radiated sound power [17]. The Ball Drop System was set up in the reverberant room at the NASA Marshall Space Flight Center in Huntsville, Alabama. Sound pressure was measured at 10 points in the room while balls were periodically hitting the plate. The sound pressure measurements were statistically aggregated; the mean sound pressure was then related to the sound power through the measured decay rate of the room [17,13]. The decay rate was determined from four measured sound pressure decay histories that were excited by an explosive charge. Decay rates were fitted to envelopes of the decay histories obtained by dividing the decay into time intervals and forming the mean square pressure in each interval. The four resulting decay rates were then statistically combined. The error bars in

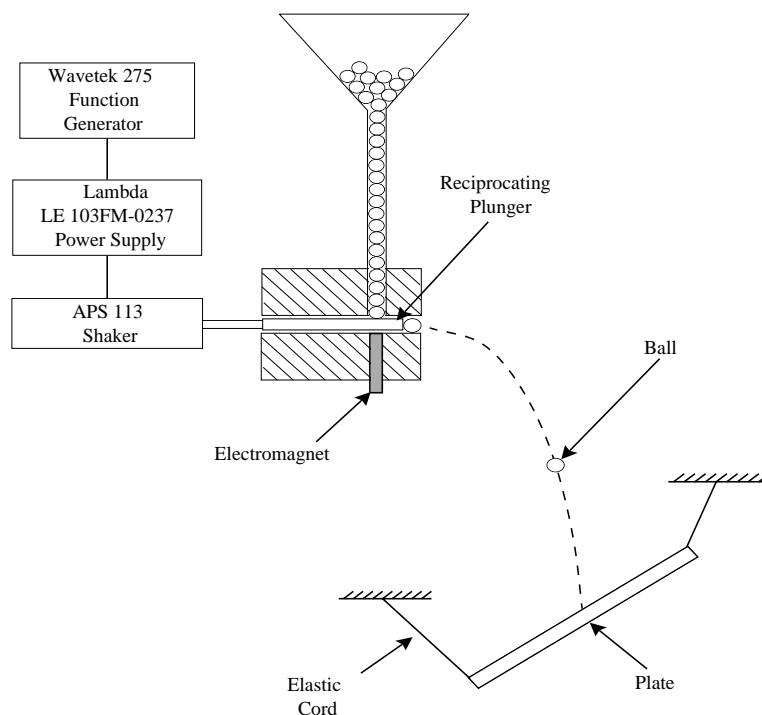


Fig. 3. Schematic of Ball Drop System.

the plots below are equal to one standard deviation of the mean and express uncertainty due to variations in spatial sound pressure and decay rate.

3.1. Analysis

The simplicity of the Ball Drop System lends itself to simple closed form analysis. The coupled analysis of the Ball Drop System with a flexible baseplate is only moderately more complicated than the decoupled analysis with a rigid baseplate. For this reason, the decoupled analysis of the Ball Drop System is presented as a limiting case of the coupled analysis.

In the framework of the methodology, the balls comprise the mechanism and the plate comprises the support structure. The ball is modelled as a point mass because its fundamental period of vibration is much shorter than the duration of impact. The plate is modelled as a single subsystem of plate bending modes. The elastic cords are neglected since the resonant frequency of the plate bouncing on the cords is well below audible frequencies. The plate is represented as a mobility element with response function $y(t) = \delta(t)/R_\infty$, where $R_\infty = 4\rho c_l h^2/\sqrt{3}$ is the modal-average drive point resistance of a plate in which ρ , h , and c_l are the density, thickness, and bulk speed of the plate [3]. The ball and plate interact through an impact force normal to the plate. The deformation near the contact point between the ball and plate is modelled by a linearized Hertzian contact stiffness of 30×10^6 N/m [13]. Applying Eqs. (1) and (15) gives a differential equation for impact force Q between the ball and plate,

$$\ddot{Q} + 2\zeta\omega_b\dot{Q} + \omega_b^2Q = 0, \quad (18)$$

where $\omega_b = \sqrt{k/m}$ is the bounce frequency of a ball against a very thick plate that deforms only near the contact point (14.6 kHz for the Ball Drop System), and $\zeta = \sqrt{km}/2R_\infty$ is a rebound indicator; balls rebound when $\zeta > 1$. The force pulse due to one impact is obtained by solving Eq. (18) subject to initial conditions of $Q(0) = 0$ and $\dot{Q}(0) = kv_0$ in which v_0 is the ball impact velocity, and zeroing the force once contact is lost. The one-sided spectral density $W_\Pi(f)$ of power delivered to the plate can be found from the periodic train of these force pulses [9]:

$$W_\Pi(f) = 2v|\mathcal{Q}(2\pi f)^2|/R_\infty, \quad (19)$$

in which v is the rate at which balls collide with the plate, and $\mathcal{Q}(\omega)$ is the Fourier Transform of the force pulse $Q(t)$:

$$\frac{\mathcal{Q}(2\pi f)}{(mv_0)^2} = \begin{cases} \frac{4e^{-\pi\beta}|\cos[(\pi/2)(\Omega_d - i\beta)]|^2}{[1 - \Omega^2]^2 + 4\zeta^2\Omega^2}, & \zeta < 1, \\ \frac{1}{[1 - \Omega^2]^2 + 4\zeta^2\Omega^2}, & \zeta \geq 1, \end{cases} \quad (20)$$

where $\Omega = 2\pi f/\omega_b$, $\Omega_d = \Omega(1 - \zeta^2)^{-1/2}$, and $\beta = \zeta(1 - \zeta^2)^{-1/2}$. The mean square velocity of the plate is then found by Statistical Energy Analysis. With the assumption of negligible acoustic damping, the mean square velocity of the plate of the Ball Drop System takes a simple form: $\langle v^2 \rangle = \int_{\Delta f} W_\Pi(f)df/(2\pi f_c \eta M)$, where η and M are the modal average loss factor and mass of the

plate, Δf is the analysis bandwidth, and f_c is the band center frequency. The plate radiation is then found using Eq. (11). The noise radiation from the balls is neglected because of a small 0.0048 ball-to-plate surface area ratio. A radiation efficiency for un baffled plates is used since the plate is not based by any surrounding structures [18].

Decoupled analysis of the Ball Drop System is obtained as a limiting case of the coupled analysis by allowing the plate thickness to increase without bound, $\zeta \rightarrow 0$.

3.2. Coupling criterion

The coupling criterion involves a ratio of mechanism and support energies evaluated during impacts and based on decoupled analysis. Due to the duration and timing of the impacts and the rate of vibration energy dissipation, less than 3% of the impact energy is dissipated during impact and less than 10^{-5} of the plate energy delivered by the previous impact remains when the next impact occurs. Therefore, the plate energy obtained by applying the rigid base impact force to the flexible plate, required by the coupling criterion, is well approximated by $E_{supp} \approx (1/R_\infty) \int_0^{\pi/\omega_b} [\sqrt{km}v_0 \sin \omega_b t]^2 dt = \pi\zeta mv_0^2$ in which the bracketed quantity is the impact force of a ball on a rigid base. The total kinetic and potential energy of a bouncing ball during impact is $E_{mech} = mv_0^2/2$, since a rigid base does not draw energy from the ball. The coupling ratio therefore is $\langle E_{supp} \rangle / \langle E_{mech} \rangle = 2\pi\zeta$.

3.3. Results

Predictions and measurements of A-weighted radiated sound power in one-third octave bands are compared in Figs. 4 and 5 for the 6.4 mm and 12.7 mm thick plates. The figures show that radiated sound power is more accurately predicted at high frequencies than low frequencies. One-third octave band levels predicted by coupled analysis are typically within 5–8 dB of measured values at the lowest frequencies for both plate thicknesses. Accuracy generally improves with frequency, and consistent 3 dB accuracy occurs when the one-third octave band mode count in the plate reaches three; this happens at 2000 Hz for the thin plate and at 4000 Hz for the thick plate. The sawtooth feature of the measured radiation and the erratic prediction accuracy below these transition frequencies is due to a low density of resonant modes in the plate. The average one-third octave band mode counts fall below unity at roughly 630 Hz for the 6.4 mm plate and at 1250 Hz for the 12.7 mm plate. One-third octave bands below these frequencies are likely to contain one or no resonating plate modes, but the modelling scheme, which statistically considers only resonant behavior, allocates a fraction of a resonant mode in each band. Without resonant modes, sound is radiated from non-resonant plate motion like the structural near field about the impact point [19], and radiation falls to a local minimum below the mean predicted value. With one resonant plate mode, the radiation peaks above the mean predicted value.

The low frequency predictions in Figs. 4 and 5 are biased high by roughly 5 dB, indicating that the analysis fails to describe some phenomena. The modal average plate description and un baffled plate radiation efficiency, which are derived for simply supported boundary conditions, do not exactly describe the behavior of each mode of the free plate like acoustic coupling between radiating regions and spatial drive point dependence. Impact near a nodal region of the free plate,

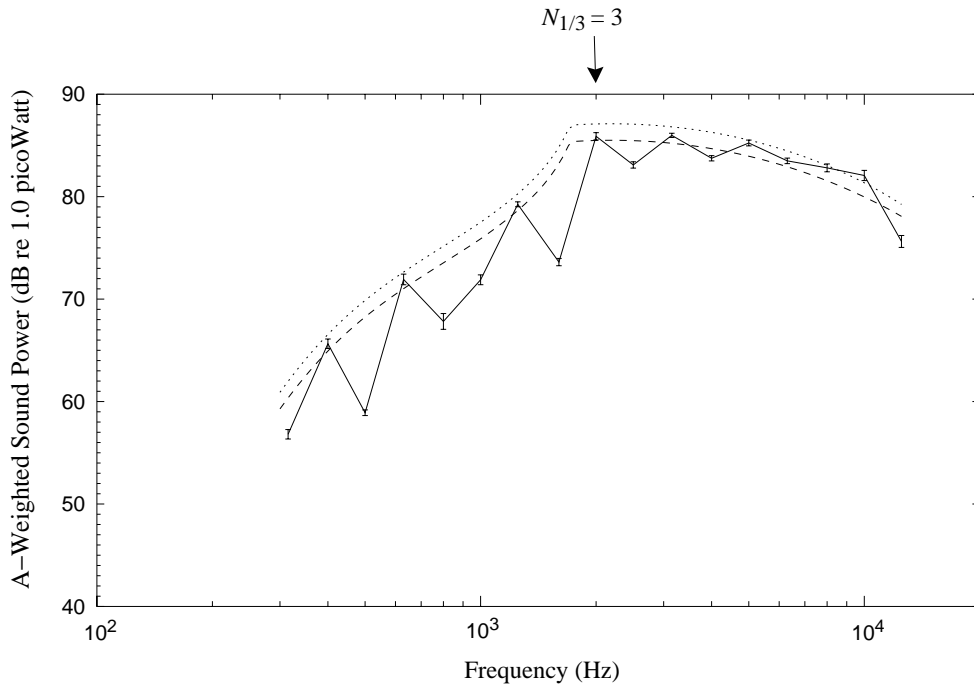


Fig. 4. Measured and predicted sound power spectra for the Ball Drop System with a 6.4 mm thick plate: —, measured; ---, coupled; · · ·, decoupled. Frequency above which one-third octave band mode count $N_{1/3}$ exceeds three is indicated.

for example, would reduce the power accepted and radiated by the plate relative to the modal-average prediction.

In spite of the bias in the low-frequency bands, prediction accuracy of overall A-weighted radiated power does not suffer terribly because band level predictions are best in the high frequency bands that dominate sound radiation. Coupled analysis predicts overall sound power within 2 dB for both plates, as shown in Table 1.

The coupling criterion values listed in Table 1 are below unity and suggest that dynamic coupling between the balls and plate has a weak effect on radiated sound. The closeness of the radiated powers predicted by coupled and decoupled analysis, which are less than 2 dB apart, confirms weak coupling. Coupled analysis gives lower sound power predictions because smaller impact forces are developed against the flexible base of coupled analysis than the rigid plate of decoupled analysis.

The results of the Ball Drop System have shown that the methodology predicts noise radiation with useful engineering accuracy, especially at the high-frequency bands that contain high mode counts and the bulk of sound radiation. The coupling criterion has passed its first test of indicating coupling strength, based only on a decoupled rigid base analysis, which neglects this coupling. The same conclusions, and some others, are drawn from the Impact Beam System considered in the next section.

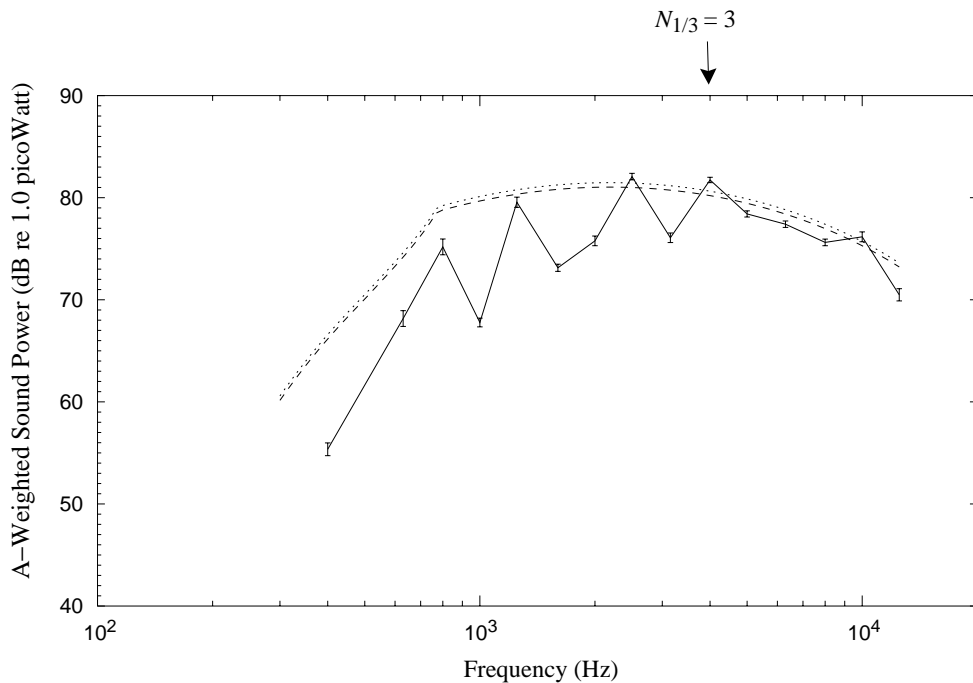


Fig. 5. Measured and predicted sound power spectra for the Ball Drop System with a 12.7 mm thick plate: —, measured; ---, coupled; · · ·, decoupled. Frequency above which one-third octave band mode count $N_{1/3}$ exceeds three is indicated.

Table 1
Performance of the coupling criterion for the Ball Drop System

Plate thickness (mm)	Coupling criterion	Overall sound power (dB(A))		
		Measured	Coupled analyses	Decoupled analysis
6.4	0.80	93.7	93.9	95.5
12.7	0.20	88.8	90.7	91.1

4. The Impact Beam System

The Impact Beam System provides another test of the methodology on a more complex system than the Ball Drop System. The Impact Beam System is pictured in Fig. 6. Its primary member is a beam hinged by a flexure on one end and constrained by a clearance bearing at the other. The two sides of the clearance bearing each contain a hemispherical steel cap backed by a piezoceramic element that senses dynamic impact force. The beam is mounted on a $0.4 \text{ m} \times 0.32 \text{ m} \times 6.4 \text{ mm}$ baseplate which is supported by four legs mounted on a plywood base that is isolated from the floor by foam. The beam is sinusoidally driven by a shaker and a connecting rod.

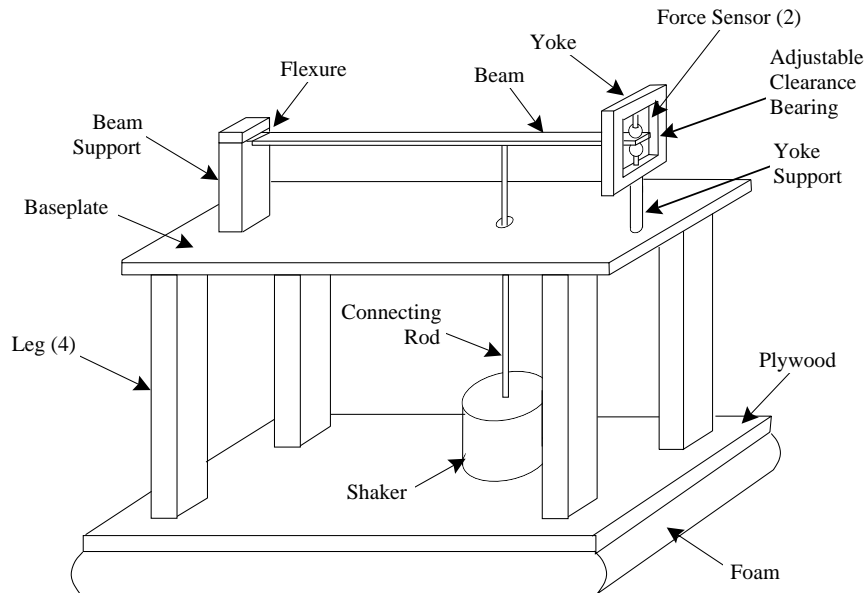


Fig. 6. The Impact Beam System.

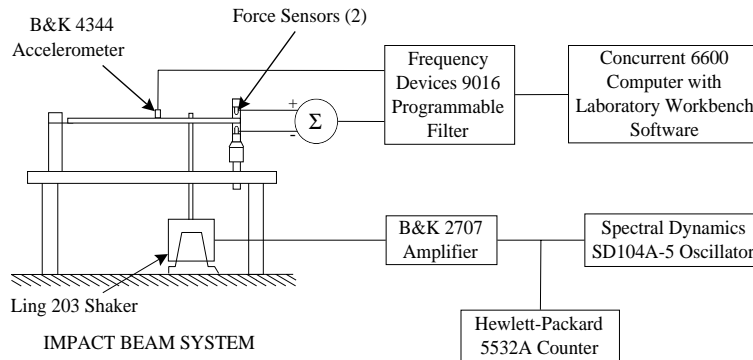


Fig. 7. Instrumentation for component vibration and bearing force measurement.

Bearing forces and system vibration were measured during system operation using the instrumentation shown in Fig. 7. Sound power was measured using the sound intensity method [17]. An intensity probe was swept over a control surface consisting of a dowel frame cross woven with string. The string divided the control surface into equal subareas, and an equal amount of time was spent sweeping over each area to promote an unbiased measurement. The sweep rate was kept slow, such that the distance moved by the probe during measurement time was much smaller than the shortest acoustic wavelength of interest. Intensity measurements were repeated until the standard deviation of mean overall intensity level, summed over frequency and the subareas, was less than 0.5 dB; this required 3–5 sweeps. Sound power was then obtained by multiplying the summed intensity spectrum by the area of the control surface. Plots of sound power and other

dynamic variables in this section show error bars that represent one standard deviation of the mean.

Loss factors for the Impact Beam System were obtained experimentally with the Impact Beam System assembled and were used as model parameters. Measured loss factors for the assemblage consisting of the beam, connecting rod, and shaker range from 0.006 to 0.1 over frequency, the high values arising from electrical losses in the shaker coil; loss factor values for the assembled yoke, yoke support, beam support, and baseplate range from 0.005 to 0.01.

4.1. Analysis

Following the framework of the methodology, the impact beam system is partitioned. The yoke, yoke support, beam support, and baseplate comprise the mechanism, and the baseplate comprises the support structure. The legs supporting the baseplate are assumed dynamically and acoustically unimportant and are not modelled. The baseplate is represented as a plate bending subsystem. The mechanism and support interact at a pair of mechanism coupling nodes and a pair support ports that are joined together; see Fig. 8. Only vertical interactions are considered. Noise radiated by the yoke, yoke support, and beam support is neglected.

The methodology is implemented using the simple and numerical modelling approaches. The simple approach involves extensive idealizations to allow application of the closed form expressions used for the Ball Drop System to the Impact Beam System. The numerical approach uses finite element descriptions to express the distributed mass and flexibility of the Impact Beam System and numerical time integration to describe multiple impacts per operating cycle.

4.1.1. Numerical modelling approach

In the numerical modelling approach, the beam, beam support, yoke, and yoke support are represented as one mechanism link. A single link representation is possible because the nominal configuration of the Impact Beam System is static during operation; in other words, perturbations

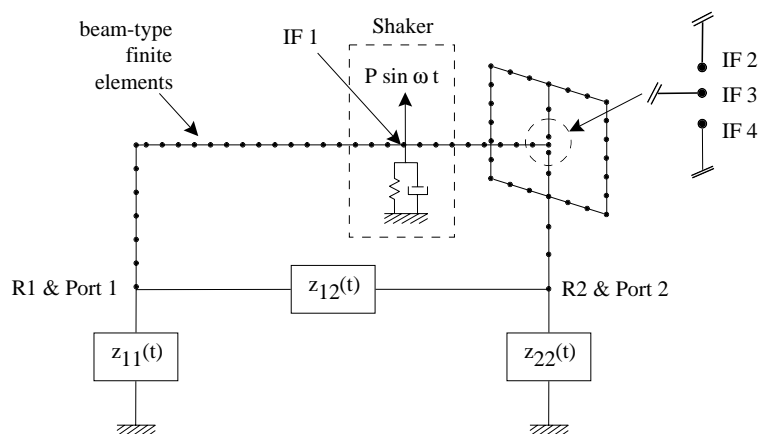


Fig. 8. Dynamic model of the Impact Beam System for coupled analysis showing finite elements, support model, shaker elements, interface (IF) nodes, and mechanism coupling (R) nodes and support ports; coupling nodes and support ports coincide.

from the nominal static configuration adequately describe system motion. A finite element representation of the single “link” was obtained using ADINA [20]. The connecting rod is represented as a point mass because its lowest resonance was experimentally found to be 70 Hz, well above the 10 Hz operating speed. The shaker is modelled as a spring and dashpot in parallel, the stiffness (4900 N/m) and resistance (32 kg/s) of which were inferred from measured natural frequency (24 Hz), loss factor (1.0), and mass (0.22 kg) of the beam-connecting rod-shaker assembly and an assumed rigid body rotation of the beam about its flexure.

The size of the finite element representation was then reduced using component mode synthesis (CMS). A study of the number of CMS vibratory modes retained in the mechanism description revealed a large change in predicted time-integrated system response when adding one CMS mode and relatively minor changes thereafter [13]. The results discussed below use a single vibratory CMS mode.

Interface loads applied to the mechanism include excitation and impact forces, which are applied to interface nodes; see Fig. 8. The electromagnetic shaker force on the shaker coil is applied to interface node 1. The amplitude of this sinusoidal force (7.6 N) was determined from current measurements and the shaker’s force–current constant. Impact forces between the beam and the instrumented clearance bearing are related to the relative motion between the beam end and the bearing:

$$Q_3 = \begin{cases} -\max[k_b(q_2 - q_3) + r_b(\dot{q}_2 - \dot{q}_3), 0], & q_2 - q_3 > \delta/2, \\ 0, & \text{otherwise,} \end{cases} \quad (21)$$

$$Q_4 = \begin{cases} \max[k_b(q_4 - q_2) + r_b(\dot{q}_4 - \dot{q}_2), 0], & q_4 - q_2 > \delta/2, \\ 0, & \text{otherwise,} \end{cases} \quad (22)$$

$$Q_2 = -(Q_3 + Q_4), \quad (23)$$

in which the function $\max()$ returns the maximum of its arguments and guarantees repulsive impact forces; q_i , \dot{q}_i and Q_i are the vertical displacements, velocities and forces at interface node i ; δ is the bearing clearance; and $k_b = 16 \times 10^6$ N/m and $r_b = 5.3$ kg/s are the bearing stiffness and resistance from a linearized Hertzian contact analysis with an assumed bearing loss factor of 0.001 [13]. The mechanism interacts with the support structure at two vertical d.o.f., one under the beam support and the other under the yoke support; see Figs. 6 and 8. Sound power radiated by the beam is obtained using radiation efficiencies for beams [21,22]. Sound power radiated by the baseplate was obtained using a radiation efficiency for plates [23]. A baffled plate model is used because the scattering length of the beam support, yoke support, and four legs is on the order (one-fourth) of the perimeter of the baseplate.

For decoupled analysis, a 2×2 mobility matrix describes the baseplate, following Eq. (7). The stiffness matrix \mathbf{K} was obtained by finite element analysis, and the modal average mobility matrix $\tilde{\mathbf{Y}}_\infty$ is obtained from an infinite plate model, with elements

$$\tilde{Y}_{ij}(\omega) = \frac{1}{R_\infty} [H_0^{(1)}(k_b r_{ij}) - H_0^{(1)}(ik_b r_{ij})], \quad (24)$$

in which R_∞ is the drive point resistance of an infinite plate, $H_0^{(1)}$ is the Hankel Function of the First Kind, r_{ij} is the distance between port d.o.f., and $k_b = (\omega/\kappa c_\ell)^{1/2}$ is the plate bending wave number, where κ and c_ℓ are the radius of gyration and bulk speed of the baseplate.

For coupled analysis, the inertia at the coupling nodes of the mechanism provided by the finite element description allows an impedance representation for the baseplate. The impedance response functions are obtained by approximately inverting and then Fourier transforming a matrix of subsystem mobilities to give an analytic expression of the impedance response functions in three steps. First, an element of an impedance matrix is decomposed:

$$\tilde{Z}_{ij} = \left. \frac{\tilde{L}_i}{\tilde{V}_j} \right|_{\substack{\tilde{v}_k=0, \\ k \neq j}} = \left[\left(\frac{\tilde{L}_j}{\tilde{V}_j} \right) \left(\frac{\tilde{L}_i}{\tilde{L}_j} \right) \right]_{\substack{\tilde{v}_k=0, \\ k \neq j}} = \tilde{Z}_{jj} \left(\frac{\tilde{L}_i}{\tilde{L}_j} \right)_{\substack{\tilde{v}_k=0, \\ k \neq j}}. \quad (25)$$

Then the force ratio is evaluated using reciprocity [3]:

$$\left. \frac{\tilde{L}_i}{\tilde{L}_j} \right|_{\substack{\tilde{v}_k=0, \\ k \neq j}} = - \left. \frac{\tilde{V}_j}{\tilde{V}_i} \right|_{\substack{\tilde{L}_j=0, \\ k \neq j}} = - \left. \frac{\tilde{Y}_{ij}}{\tilde{Y}_{ii}} \right|_{\substack{\tilde{v}_k=0, \\ k \neq i,j}}, \quad (26)$$

in which the right-hand side is a ratio of transfer and drive point mobilities with all but two port d.o.f. immobilized (clamped). Combining these expressions and relaxing the clamping condition gives $\tilde{Z}_{ij} \approx 1/\tilde{Y}_{ij}$ and

$$\tilde{Z}_{ij} \approx \begin{cases} 1/\tilde{Y}_{ii}, & i = j, \\ -\tilde{Y}_{ij}/(\tilde{Y}_{ii}\tilde{Y}_{jj}), & i \neq j. \end{cases} \quad (27)$$

The relaxation of the clamping is motivated by the weak dependence of higher order mode dynamics on boundary conditions, which weakens with increasing frequency [24,25,3]. The accuracy of this approximation is assessed by evaluating drive point and transfer impedances for an infinite plate. The infinite plate mobilities given by Eq. (24) are inverted exactly and approximately by Eq. (27). The approximation is within 10% for separations exceeding a wavelength, $k_b r_{ij} > 2\pi$, as seen in Fig. 9. Similar behavior is expected for modally dense finite systems because of the previously described infinite system analogy. Evaluating Eq. (27) gives impedance response functions for a plate subsystem [26,13]:

$$z_{ij}^\infty(t) = \begin{cases} R_\infty \delta(t), & i = j, \\ -\frac{2}{\pi} R_\infty \left\{ \left[\frac{\pi}{2} - F(\alpha_{ij}) \right] \delta(t) - \left[\frac{\partial}{\partial t} F(\alpha_{ij}) \right] u(t) \right\}, & i \neq j, \end{cases} \quad (28)$$

in which $F(\alpha_{ij}) = \int_0^{\alpha_{ij}} (\sin x/x) dx$ and $\alpha_{ij} = r_{ij}^2/(4\kappa c_\ell t)$, where r_{ij} is distance between the source point j and the receiving point i , $\delta(t)$ is the delta function, and $u(t)$ is the unit step function.

4.1.2. Simple modelling approach

The simple approach involves a number of idealizations to allow application of closed form expressions to the Impact Beam System. Numerical integration of a nonlinear dynamic system is avoided by asserting that two well-defined impacts occur per shaker cycle, on the bottom and top bearings, near times when the applied shaker force is zero. Further idealizations are that the

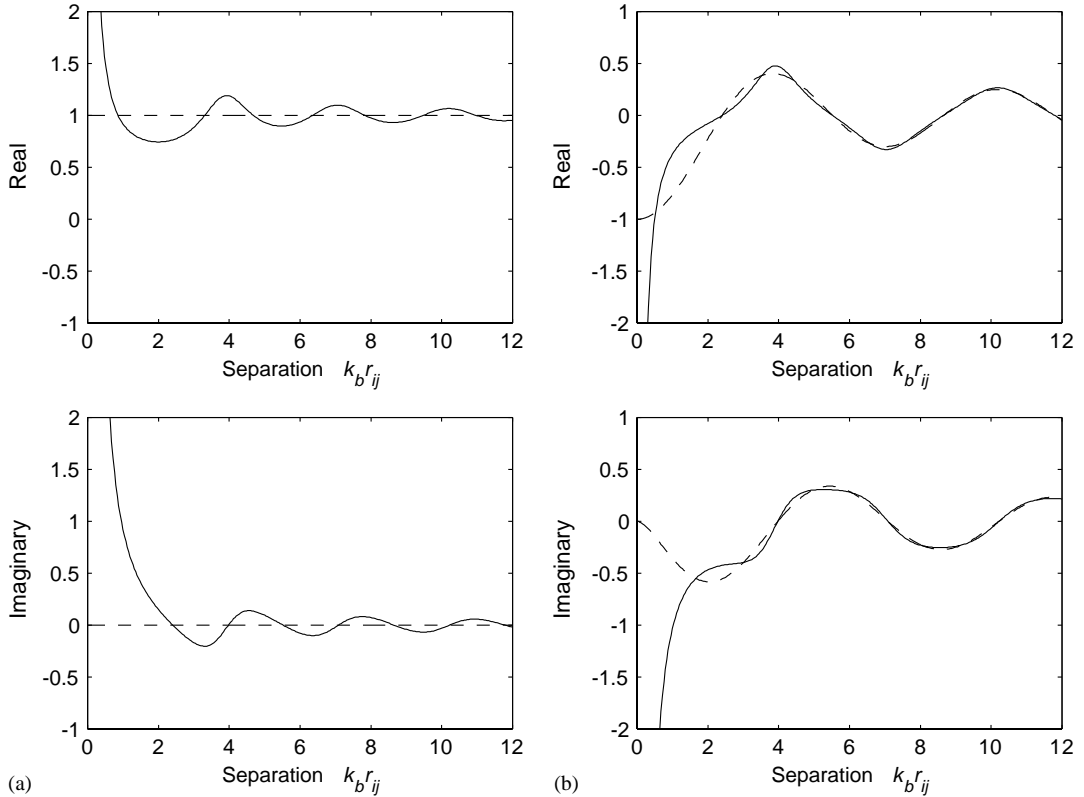


Fig. 9. Comparison of approximate and exact (a) drive point impedance Z_{ii} and (b) transfer impedance Z_{ij} , normalized by the infinite plate drive point impedance R_{∞} for dimensionless separation $k_b r_{ij}$: —, exact; · · ·, approximate.

bearing surfaces do not move prior to beam impact; the beam, pushrod, and shaker coil move as a rigid assemblage because the shaker forcing frequency is well below the first resonance of the assemblage; the shaker force changes linearly with time when the force is near zero; the baseplate dominates radiation due to its large surface area; and structural damping far exceeds radiation damping. With these idealizations, the Impact Beam System is modelled as a mass, stiffness, and dashpot. The mass (0.11 kg) represents the rigid body rotation of the beam, pushrod, and shaker coil assemblage about the beam flexure. The stiffness (30×10^6 N/m) represents Hertzian contact between the beam and bearing. The dashpot (1280 kg/s) represents the multi-bending mode behavior in the baseplate. The velocity just before impact is found by assuming that the rigid assemblage is at rest against one bearing surface before the shaker force moves it across the clearance. The shaker force is linearized as $P\Omega t$, where P is the shaker force amplitude, Ω is the operating speed in radians/s, and t is time. Time integrating the transient response controlled largely by the beam mass gives $z = P\Omega t^3/6m$ where m is the effective mass of the assemblage. Impact velocity is found by solving this relationship for the time of impact and inserting the result into an expression for velocity, giving $v_0 = 1.65(P\Omega/m)^{1/3}\delta^{2/3}$ in which δ is clearance. Since the kinetic energy of the assemblage at impact is proportional to the square of velocity and the rate of

impacts is proportional to operating speed, the power delivered to the structure and the power radiated as sound is proportional to $\delta^{4/3}$ and $\Omega^{5/3}$. The remaining calculations of impact force, baseplate velocity, and radiated power are identical to the coupled analysis of the Ball Drop System.

4.2. Coupling criterion

The coupling criterion is evaluated using the results of decoupled analysis obtained by the numerical modelling approach. Response of the coupled and decoupled models was time integrated using Gear's method [27]. Two 10 Hz operating cycles were simulated. Start-up transients were allowed to settle during the first cycle before writing dynamic variables for the disk every 16 μ s during the second cycle. The decoupled dynamic model had 25 d.o.f.; the coupled model had 37 d.o.f. Computation time was the equivalent of less than 5 min for the decoupled model and less than 15 min for the coupled model on a modern workstation. Spectra were derived from the simulated response by Welch's method [11,27]. A 2048-point FFT with a 30.5 Hz resolution was used.

A coupling criterion of 480 was calculated using the time integrated results of the decoupled analysis. The large value suggests that coupling between the beam mechanism and the baseplate is important, in contrast with the Ball Drop System. Experimental and simulation results presented below confirm the importance of this coupling.

4.3. Results

Predictions of bearing force, beam response, baseplate response, and sound radiation are compared to measured data in the following. Predictions are made by decoupled (rigid base) and coupled analysis using the ASSET numerical modelling approach [8] to describe the clearance bearing, distributed mass, and flexibility of the Impact Beam System, along with combined elastic and modal average descriptions of the baseplate. In addition, the simple modelling approach with mechanism-support coupling included is implemented by making the simplifying idealizations described above. The sensitivity of measured and predicted overall sound radiation to operating speed, bearing clearance, and baseplate thickness is also examined.

4.3.1. Bearing force

Forces between the beam and clearance bearing were measured with specially made piezoceramic force sensors at the upper and lower bearings. The force sensors contain piezoceramic elements located directly behind steel hemispheres that can contact the beam. Measured forces at the upper and lower bearings were summed together, as shown in Fig. 7.

Measured and predicted summations of upper and lower bearing force spectra are shown in Fig. 10. The decoupled predictions are larger because the rigid base of decoupled analysis effectively stiffens the system. The decoupled force spectra are generally 3 dB less accurate, indicating that baseplate coupling has a minor effect on bearing force.

The coupled and decoupled predictions capture the general trend of the force spectrum, and accuracy tends to increase with frequency. Below 2000 Hz accuracy typically ranges from 5 to 10 dB; at and above 2000 Hz accuracy is within 5 dB. Missing features in the simulated bearing

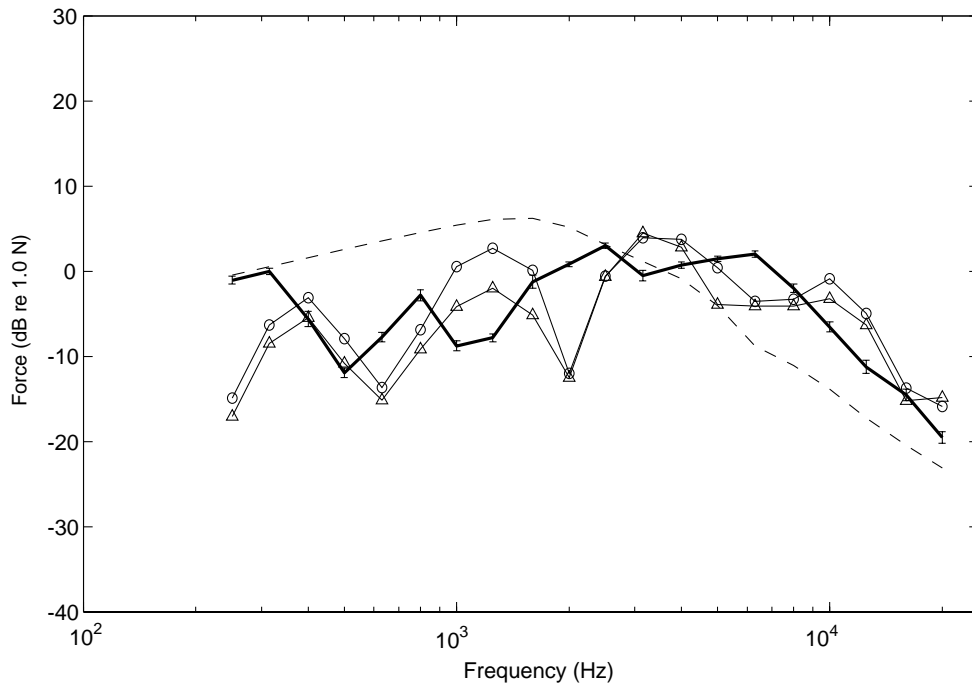


Fig. 10. Measured and predicted bearing force spectra for the Impact Beam System: —■—, measured; —△—, coupled analysis; —○—, decoupled analysis; ----, simple analysis.

force, especially at low frequencies, arise from unmodelled dynamic phenomena, most probably in the mechanism model, which has the most direct effect on bearing force. In addition, chaotic response variations present in the non-linear Impact Beam System may not be captured in the two operation cycles that were simulated [28].

The bearing force predicted by the simple analysis is less accurate than that of the coupled and decoupled analysis. Simple predictions are high below 3000 Hz and low above 3000 Hz. Accuracy suffers because of the neglect of multiple impacts and rattling associated with rebounds. Multiple impacts on both sides of the bearing reduce the summed bearing force at low frequencies by partial cancellation but tend to increase the force spectrum by summing incoherently at high frequencies.

4.3.2. Beam vibration

Surface normal acceleration was measured at six points on the beam, time integrated, squared, and spatially averaged to obtain mean square velocity. Beam nodal velocities produced by coupled and decoupled simulations were similarly processed. The beam velocity of simple analysis is obtained by dividing the impact force by radian frequency and the effective mass of the beam assembly, which is assumed rigid. The beam velocity results in Fig. 11 are similar to the bearing force results in terms of the relationship between the measured, coupled, decoupled and simple values. Coupled and decoupled predictions usually differ by less than 3 dB, and mechanism support coupling has a small effect on beam response. The notable difference between the bearing force and beam vibration results is the behavior in the 16 and 20 kHz bands, where bearing force is

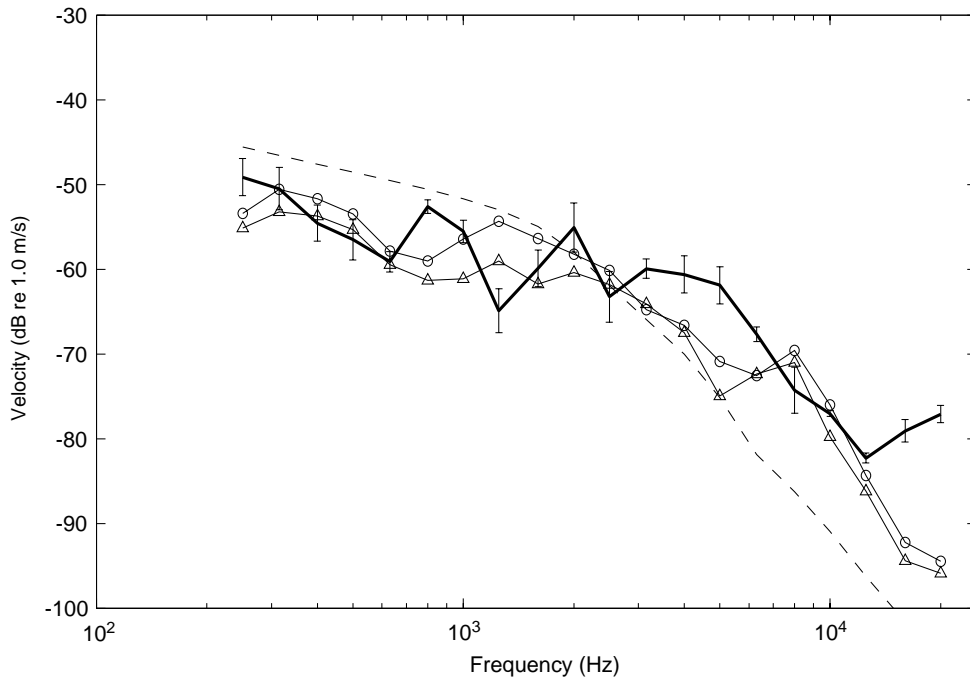


Fig. 11. Measured and predicted beam vibration spectra for the Impact Beam System: —, measured; —△—, coupled analysis; —○—, decoupled analysis; ---, simple analysis.

over-predicted by 4 dB but beam vibration is under-predicted by 12–18 dB. This is probably due to unmodelled longitudinal resonant behavior in the beam vibration support and yoke fixture. The beam results also differ in that the coupled and decoupled analysis, and to some extent the simple analysis, usually predict beam vibration more accurately than bearing force below 16 kHz, suggesting that beam response is less sensitive to system parameters than bearing force. Offsetting dynamic effects may be responsible for this result: system resonance reduces dynamic stiffness and therefore bearing force, but the resonance also increases beam response to a given amount of bearing force.

4.3.3. Baseplate vibration

Surface normal acceleration was measured at 12 points on the baseplate, integrated, squared, and averaged to obtain mean square velocity. Baseplate vibration results are shown in Fig. 12. There is similarity to the bearing force and beam vibration results in that the decoupled predictions exceed coupled predictions, but the difference is substantially greater, usually more than 10 dB. The large disparity indicates that baseplate response is quite sensitive to mechanism-support coupling. This result is consistent with the coupling criterion, which suggests the importance of this coupling. The coupled predictions, which include the coupling, are generally 5–15 dB more accurate than the decoupled predictions. The simple analysis gives mixed performance with accuracies worse than decoupled analysis below 2000 Hz, accuracies between decoupled and coupled analysis at 2000–4000 Hz, and accuracies comparable to coupled analysis above 4000 Hz.

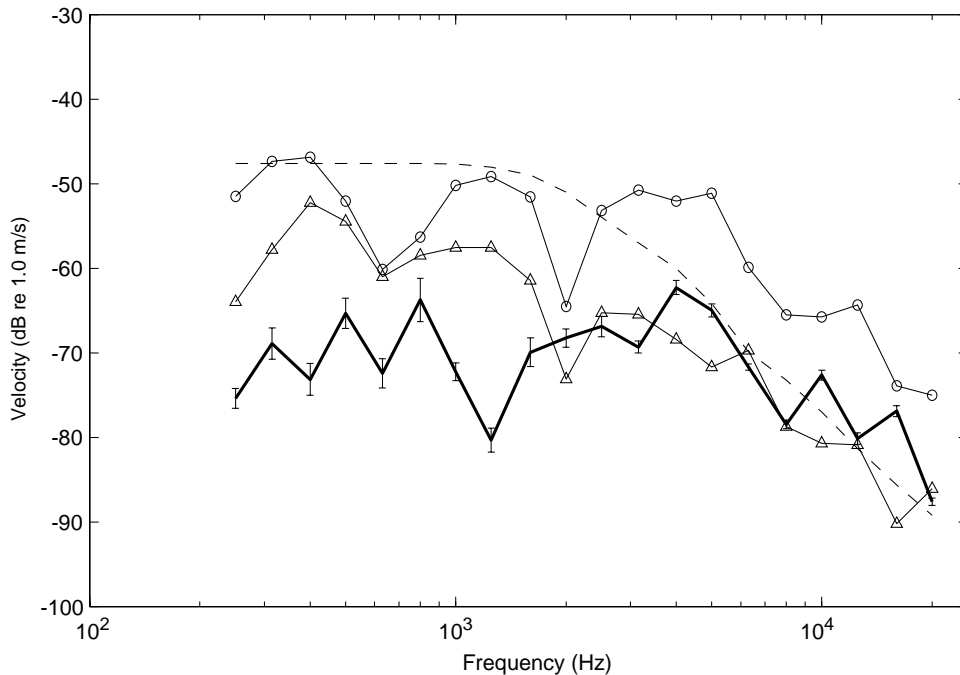


Fig. 12. Measured and predicted baseplate vibration spectra for the Impact Beam System: —, measured; —△—, coupled analysis; —○—, decoupled analysis; ---, simple analysis.

The accuracy of coupled analysis varies substantially with frequency, and it is interesting to consider the baseplate description, which contains stiffness and resistance terms. Equal elastic and resistive forces result from baseplate motions at 750 Hz, elastic effects dominate below 750 Hz, and resistive effects above 750 Hz. Since coupled predictions exceed measured values by more than 10 dB below this frequency, the elastic description is clearly lacking some important dynamic details. In the 800–1600 Hz range resistive effects dominate, but the baseplate mode count is too low to produce reliable results. Above 1600 Hz, resistive effects dominate, the baseplate mode count exceeds three, and predictions are generally within 3–5 dB of measured values.

4.3.4. Sound radiation

Measured and predicted A-weighted sound power is compared in Fig. 13. The relations between the coupled, decoupled, simple, and measured results are similar to those of baseplate vibration. Decoupled predictions usually exceed coupled predictions by more than 10 dB, further confirming the importance of mechanism-support coupling and the ability of coupling criterion. Consistent accuracy is again achieved when the baseplate mode count exceeds three.

The similarity of the sound power and baseplate results suggests that the baseplate dominates sound radiation. To check this, the sound power contributions of the beam and baseplate are inferred from measured surface normal velocities and the radiation efficiencies used in the methodology. Inferred and measured sound powers are shown in Fig. 14. The closeness of the baseplate contribution to the measured data confirms the dominance of the baseplate.

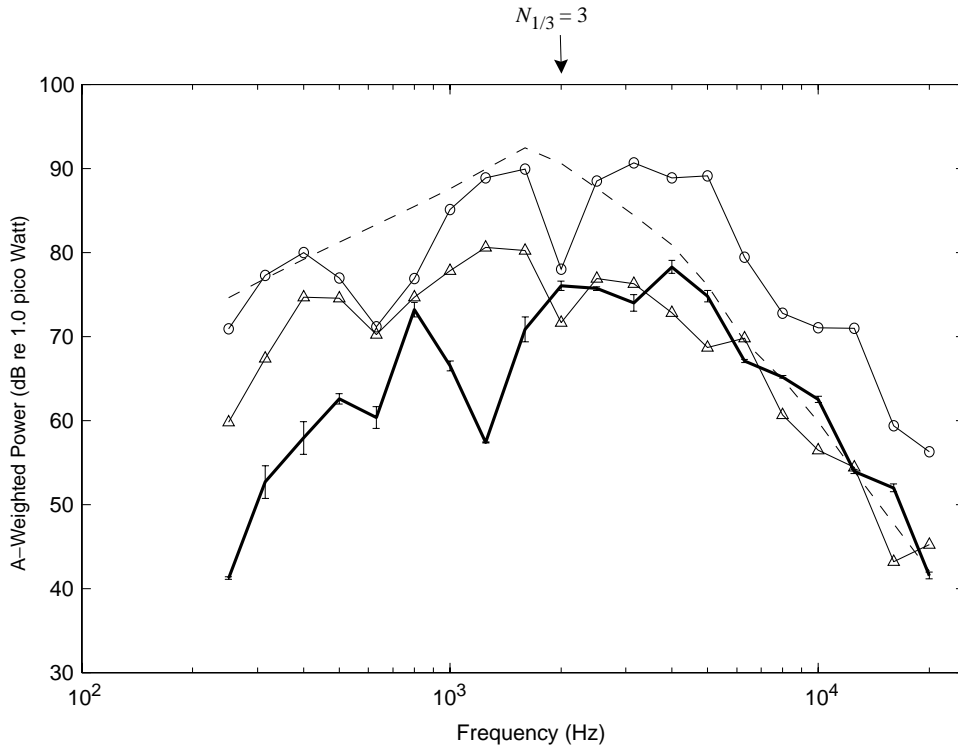


Fig. 13. Measured and predicted sound power spectra for the Impact Beam System: —, measured; —△—, coupled analysis; —○—, decoupled analysis; ---, simple analysis. Frequency band above which one-third octave band mode count $N_{1/3}$ exceeds three is indicated.

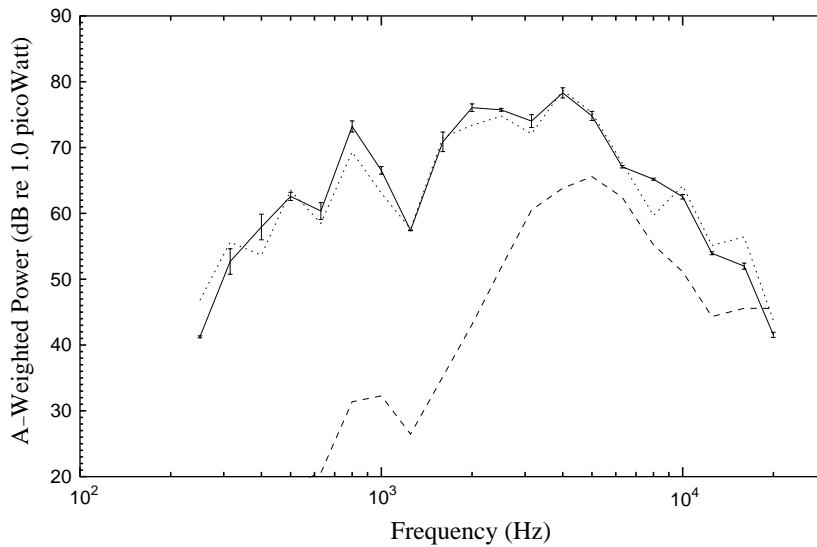


Fig. 14. Sound power of Impact Beam System: —, measured; ---, inferred from measured beam vibration; · · ·, inferred from measured plate vibration.

The overall A-weighted sound power is predicted relatively well, within 3.5 dB, by coupled analysis in spite of relatively poor band level accuracy below 2000 Hz. This occurs because the baseplate radiates most efficiently above its critical frequency of 2000 Hz, and A-weighting deemphasizes low-frequency radiation.

4.3.5. Parametric noise trends

The variation of overall radiated sound power with changes in operating speed, bearing clearance, and baseplate thickness is now discussed. The parameter range considered is 2–40 Hz operating speed, 0.076–2.03 mm clearance, and 3.2–12.7 mm baseplate thickness. One parameter was varied at a time from a baseline setting of 10 Hz operating speed, 0.51 mm clearance, and a 6.4 mm baseplate thickness. Predictions by coupled and simple analyses are compared to measured data in Figs. 15–17.

The coupled and simple analyses predict overall radiation trends with comparable accuracy. The simple analysis better predicts the speed trend, while the coupled analysis better predicts the clearance trend. Neither method produces the observed monotonically decreasing thickness trend, which indicates that with increasing thickness the reduction in plate vibration more than offsets the increase in radiation efficiency. Although trends are predicted comparably, the coupled predictions are generally 8–14 dB more accurate than simple predictions and are within 3–5 dB of the measured data at all but the largest values of clearance and speed. Unlike simple analysis, coupled analysis predicts the observed breaks in the increasing trends of speed and clearance. The breaks occur when the sinusoidal shaker force departs substantially from a linear profile before the beam traverses the clearance and impacts a bearing surface. In the limit of very high speed or very large clearance no impacts would occur because the beam tip displacement would be less than the clearance.

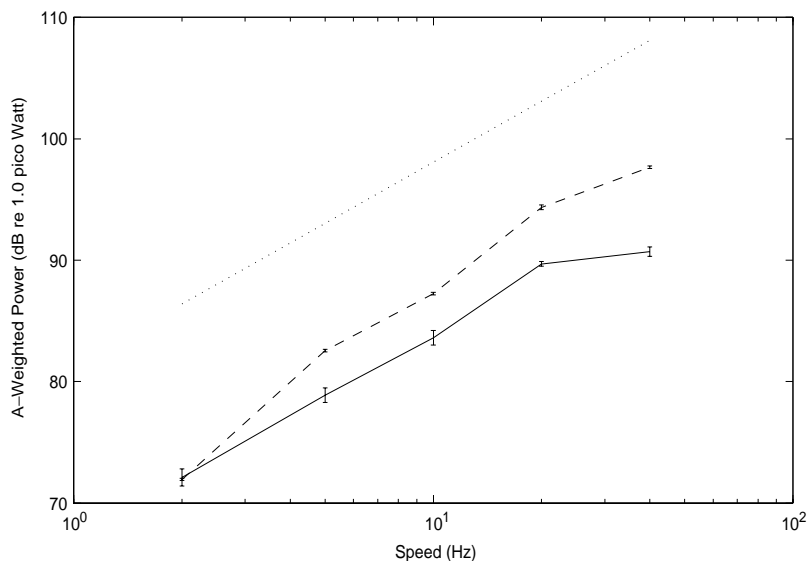


Fig. 15. Measured and predicted overall A-weighted sound power variation with operating speed: —, measured; ---, coupled analysis; · · ·, simple analysis.

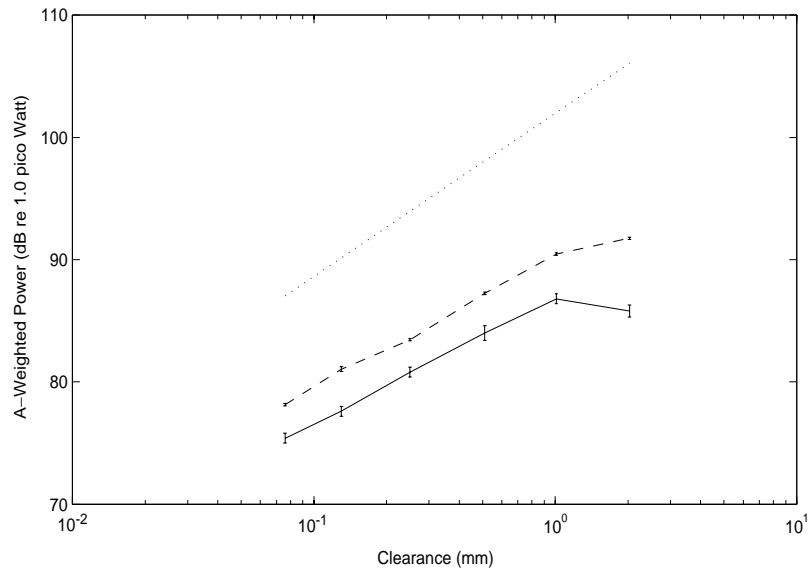


Fig. 16. Measured and predicted overall A-weighted sound power variation with bearing clearance: —, measured; ---, coupled analysis; · · ·, simple analysis.

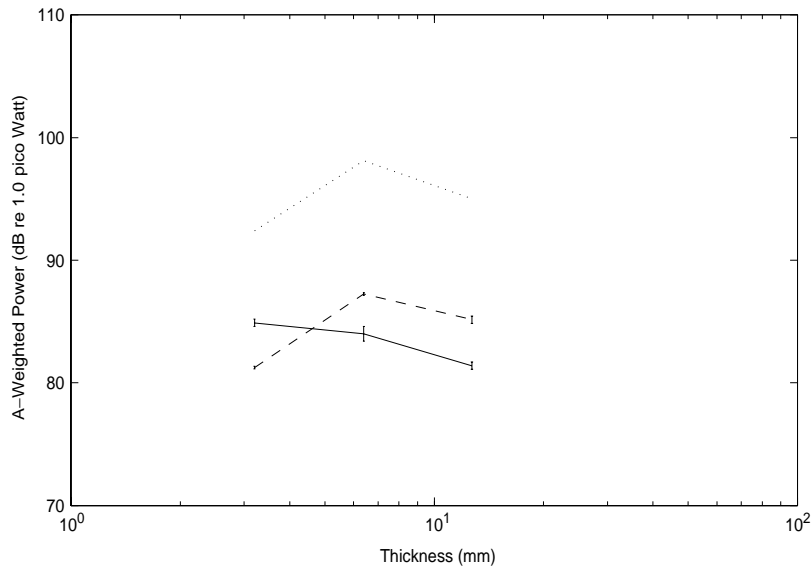


Fig. 17. Measured and predicted overall A-weighted sound power variation with baseplate thickness: —, measured; ---, coupled analysis; · · ·, simple analysis.

5. Conclusions

A methodology for predicting noise radiation caused by impacts in machine systems consisting of mechanisms and their support structures has been developed and tested against measurements

of two mechanical systems. The methodology predicts noise and vibration, ranks noise contributions, and assesses noise trends due to system parameter variations. The methodology uses a heuristic energy-based coupling criterion to indicate the importance of dynamic coupling between a mechanism with nonlinear dynamic behavior and its support structure, based on a decoupled analysis of a mechanism operating on a rigid base. A coupled analysis that considers mechanism-support coupling is pursued when the coupling criterion deems the need. The coupling criterion is observed to indicate the importance of mechanism-support coupling, as well as the usefulness of the decoupled analysis. In some cases the coupling is observed to significantly affect vibration and noise radiation of the support structure, while having a relatively minor effect on the response of the mechanism. The methodology allows for flexibility in the modelling techniques used to describe mechanisms and their support structures, and two approaches have been investigated. The first is a simple closed form approach that involves substantial idealization of the machine system and prescribes a priori the number of impacts per operating cycle. The second is a numerical approach that describes the distributed mass and flexibility, time-varying kinematic configurations, and joint clearances of mechanisms and places no prescriptions on impact behavior. The simple closed form approach is found to compete with the numerical approach when predicting parametric noise trends, but the numerical approach provides better overall and band level accuracy. The simple approach may be useful during early stages of design, while the numerical approach is useful in later stages when better accuracy is needed.

The support structures of the two examined systems are hard-mounted to their mechanisms and are found to dominate noise radiation. The support structure description is therefore critical to prediction accuracy. The methodology generally provides 3–5 dB accuracy in sound power band level when the mode count of the support structure exceeds three. Larger prediction errors at lower frequencies are almost entirely due to misrepresentation of the support structure. In spite of this inaccuracy, the methodology essentially achieves its goals of predicting A-weighted sound power levels to 3 dB and providing most accurate predictions of radiated band levels in the 500–10,000 Hz band of heightened hearing sensitivity.

Acknowledgements

The authors gratefully acknowledge the support of the National Aeronautics and Space Administration under grant NGT-50364 and the National Science Foundation under grant MSM-8410530.

References

- [1] D.C. Hodgson, M.M. Sadek, A technique for the prediction of the noise field from an arbitrary vibrating machine, *Proceedings of the Institution of Mechanical Engineers Part C* 197 (3) (1983) 189–197.
- [2] A.F. Seybert, B. Soenarko, F.J. Rizzo, D.J. Shippy, An advanced computational method for radiation and scattering of acoustic waves in three dimensions, *Journal of the Acoustical Society of America* 77 (2) (1985) 362–368.
- [3] R.H. Lyon, *Theory and Application of Statistical Energy Analysis*, Butterworth-Heinemann, Newton, MA, 1995.

- [4] E.J. Richards, I. Carr, M. Westcott, On the prediction of impact noise, Part V: the noise from drop hammers, *Journal of Sound and Vibration* 88 (3) (1983) 333–397.
- [5] N.D. Perreira, S. Dubowsky, Predicting acoustical noise generation in complex mechanical systems, *American Society of Mechanical Engineers Journal Mechanical Design* 101 (2) (1979) 199–209.
- [6] N.D. Perreira, S. Dubowsky, Analytical method to predict noise radiation from vibrating machine systems, *Journal of the Acoustical Society of America* 67 (2) (1980) 551–563.
- [7] A.M. Martin, Occupational hearing loss and noise conservation, in: R.G. White, J.G. Walker (Eds.), *Noise and Vibration*, Ellis Horwood Limited, Chichester, England, 1982, pp. 781–803.
- [8] T. Kakizaki, J.F. Deck, S. Dubowsky, Modeling the spatial dynamics of robotic manipulators with flexible links and joint clearances, *American Society of Mechanical Engineers Journal Mechanical Design* 115 (4) (1993) 839–847.
- [9] R.H. Lyon, *Machinery Noise and Diagnostics*, Butterworths Publishers, Boston, 1987.
- [10] M.C. Kompella, R.J. Bernhard, Variation of structural acoustic characteristics of automotive vehicles, *Noise Control Engineering Journal* 44 (2) (1996) 93–100.
- [11] S.L. Marple, *Digital Spectral Analysis with Applications*, Prentice-Hall, Englewood Cliffs, NJ, 1987.
- [12] H.G.D. Goyder, R.G. White, Vibrational power flow from machines into built-up structures part i: introduction and approximate analysis of beam and plate-like structures, *Journal of Sound and Vibration* 68 (1) (1980) 59–75.
- [13] C.H. Oppenheimer, Impact-induced noise vibration of machine systems for design, Ph.D. Thesis, Department of Mechanical Engineering, Massachusetts Institute of Technology, Cambridge, MA 02139, September, 1992.
- [14] E.J. Richards, I. Carr, On the prediction of impact noise part x: the design and testing of a quietened drop hammer, *Journal of Sound and Vibration* 104 (1) (1986) 137–164.
- [15] R. Hickling, S.P. Marin, Enhancement of sound power of a component of a complex noise source by sound from other nearby components, *Journal of the Acoustical Society of America* 84 (1) (1988) 262–274.
- [16] S. Dubowsky, J.F. Deck, H. Costello, The dynamic modeling of flexible spatial machine systems with clearance connections, *American Society of Mechanical Engineers Journal Mechanisms Transmissions and Automation in Design* 109 (1) (1987) 87–94.
- [17] L.L. Beranek, I.L. Ver, *Noise and Vibration Control Engineering*, Wiley, New York, 1992.
- [18] C.H. Oppenheimer, S. Dubowsky, A radiation efficiency for un baffled plates with experimental validation, *Journal of Sound and Vibration* 199 (3) (1997) 473–489.
- [19] L. Cremer, M. Heckl, E.E. Ungar, *Structure-Borne Sound*, Springer, Berlin, 1973.
- [20] K.J. Bathe, *Finite Element Procedures in Engineering Analysis*, Prentice-Hall Inc., Englewood Cliffs, NJ, 1982.
- [21] R.K. Jeyapalan, E.J. Richards, Radiation efficiencies of beams in flexural vibration, *Journal of Sound and Vibration* 67 (1) (1979) 55–67.
- [22] W.K. Blake, The radiation from free-free beams in air and water, *Journal of Sound and Vibration* 33 (4) (1974) 427–450.
- [23] G. Maidanik, Response of ribbed panels to reverberent acoustic fields, *Journal of the Acoustical Society of America* 34 (6) (1962) 809–826.
- [24] P. Morse, H. Feshbach, *Methods of Theoretical Physics*, McGraw-Hill Book Co., New York, 1953.
- [25] P.W. Smith, R.H. Lyon, *Sound and structural vibration*, Technical Report NASA CR-160 Bolt, Beranek, and Newman Inc. 1965.
- [26] K.-E. Fällström, H. Gustavsson, N.-E. Molin, A. Wahlin, Transient bending waves in plates studied by hologram interferometry, *Experimental Mechanics* 29 (4) (1989) 378–387.
- [27] IMSL Houston, Texas USA IMSL User's Manual 9.2 Edition, 1985.
- [28] P. Gu, S. Dubowsky, Dinos, Chaotic vibration and design criteria for machine systems with clearance connections, *Journal of Dynamic Systems, Measurement and Control*, American Society of Mechanical Engineers Transactions, to be published.